Available online at www.sciencedirect.com
ScienceDirect
Trans. Nonferrous Met. Soc. China 35(2025) 296−312
Transactions of Nonferrous Metals Society of China
www.tnmsc.cn

Synergistic mechanism of metal ions and sodium N-oleoylsarcosinate on flotation separation of lepidolite from feldspar

Guo-yuan XIANG[1], Rui-hua FAN[1], Wen-tao ZHU[1], Wei SUN[1,2,3,4], Ren-ji ZHENG[1,2,3,4], Zhi-yong GAO[1,2,3,4]

1. School of Minerals Processing and Bioengineering, Central South University, Changsha 410083, China;
2. Key Laboratory of Hunan Province for Clean and Efficient Utilization of Strategic Calcium-containing Mineral Resources, Central South University, Changsha 410083, China;
3. Hunan International Joint Research Centre for Efficient and Clean Utilization of Critical Metal Mineral Resources, Central South University, Changsha 410083, China;
4. Engineering Research Center of Ministry of Education for Carbon Emission Reduction in Metal Resource Exploitation and Utilization, Central South University, Changsha 410083, China

Received 29 May 2023; accepted 30 January 2024

Abstract: The combined reagents of sodium N-oleoylsarcosinate (SNOS) with metal ions (Ca(II), Mg(II), Cu(II), and Pb(II)) was employed to facilitate the separation of lepidolite from feldspar. The synergistic interaction mechanism of this combined reagent was systematically investigated via contact angle measurements, AFM, FTIR, species distribution calculations, and DFT calculations. The results suggested that Ca(II) exhibited the best selectivity for activating lepidolite flotation. SNOS was chemically adsorbed on the Ca(II)-activated lepidolite surface with an adsorption energy of −1248.91 kJ/mol while a lower adsorption energy of −598.84 kJ/mol of SNOS on Ca(II)-activated feldspar was calculated. Therefore, this combination of SNOS and Ca(II) is a promising reagent scheme for the efficient recovery of lithium from aluminosilicate ore.

Key words: flotation; lepidolite; feldspar; sodium N-oleoylsarcosinate; metal ions

1 Introduction

Lithium, known for its excellent properties, finds wide applications in battery, aerospace, ceramic, medicine, and other fields [1,2]. As a result, there is an anticipated significant increase in the demand for lithium resources in the future [3]. Lepidolite is one of the primary minerals for lithium extraction [4]. Among the lepidolite ores, feldspar is a principal aluminosilicate gangue mineral [5,6]. Flotation is the most frequently used method to separate lepidolite from feldspar due to its high efficiency and low cost [7]. However, lepidolite flotation is influenced by the collectors and the metal ions in the pulp [8].

Cationic collectors used in lepidolite flotation mainly including dodecylamine [6], amidoxime [9], coco alkyl amine [10], dodecayltrimethylaminium-bromide [10], butanediyl-α,ω-bis (dimethyldodecyl-ammonium bromide) [5,10], and stearyl trimethyl ammonium chloride [11], are adsorbed onto the lepidolite surface through electrostatic attraction. Meanwhile, the anionic/cationic mixed collectors such as sodium dodecyl benzene sulfonate/dodecyl-amine [8], and sodium oleate/dodecylamine [8,12] always applied in lepidolite flotation, are co-adsorbed on the lepidolite surface through chemical

Corresponding author: Zhi-yong GAO, Tel: +86-13574892751, E-mail: zhiyong.gao@csu.edu.cn;
Ren-ji ZHENG, Tel: +86-19918938969, E-mail: zhengrj@csu.edu.cn
https://doi.org/10.1016/S1003-6326(24)66680-X
1003-6326/© 2025 The Nonferrous Metals Society of China. Published by Elsevier Ltd & Science Press
This is an open access article under the CC BY-NC-ND license (http://creativecommons.org/licenses/by-nc-nd/4.0/)

bond and electrostatic attraction together. Due to the presence of an amino group, single cationic and anionic/cationic mixed collectors have good collection capacity but poor selectivity in lepidolite flotation [6]. Furthermore, current lepidolite ore processing plants typically require desliming and coarse-grained flotation, which results in a low Li_2O concentrate grade and recovery [6,10,13]. Efficient flotation of lepidolite at its full particle size requires the development of flotation reagents that possess high collection capacity and selectivity.

The single anionic collectors, which have strong collection ability, cannot directly float lepidolite due to their predominantly negative charge throughout the whole pH range [6,8,12]. Additionally, specific metal ions can activate lepidolite without activating feldspar, suggesting high selectivity [14]. The joint use of an anionic collector and a metal ion is commonly employed in the flotation of spodumene [15], quartz [16], fluorite [17], scheelite [18], cassiterite [19], and chlorite [20]. However, this approach is not frequently utilized in lepidolite flotation due to the challenge of finding appropriate anionic collectors and metal ions. Therefore, it is crucial to conduct research and exploration to identify suitable anionic collectors and metal ions, as this holds significant importance in effectively separating lepidolite from feldspar.

Sarcosine surfactants such as sodium N-lauroylsarcosinate [21] and sodium N-secanoy-lsarcosinate [22] can be anionic fluorite flotation collectors. To our knowledge, sodium N-oleoy-lsarcosinate (SNOS) may be an ideal lepidolite collector for its three oxygen sites, which are inclined to react with metal ions. Moreover, it has a long hydrophobic chain of 21 carbon atoms and contains the —CON— group, representing high polarity and solubility. Metal ions such as Ca(II), Mg(II), Cu(II), and Pb(II), mainly originate from processing water, dissolution of minerals, and addition of reagents, etc., which have a substantial impact on mineral flotation [23]. Ca(II) has little effect on muscovite floatability when sodium oleate is used as a collector [24]. On the other hand, Mg(II) selectively improves the separation of spodumene from feldspar when α-bromododecanoic acid is used as a flotation collector [15]. Similarly, Cu(II) and Pb(II) can be adsorbed on lepidolite, further increasing its potential applications [14].

This study focuses on investigating the synergistic effects of metal ions (Ca(II), Mg(II), Cu(II), and Pb(II)) in combination with a novel collector (SNOS) through flotation tests conducted on lepidolite and feldspar. Notably, depressants were not added during the tests. The interaction mechanism between SNOS and lepidolite/feldspar, activated by the four metal ions, was further explored using various techniques such as contact angle measurements, atomic force microscope (AFM) measurements, Fourier transform infrared spectroscopy (FTIR) measurements, species distribution calculations, and density functional theory (DFT) calculations.

2 Experimental

2.1 Mineral samples and reagents

The pure lepidolite and feldspar were procured from Minas Gerais, Brazil and Shandong, China, respectively. To conduct flotation tests, the pure lepidolite and feldspar samples were crushed and ground to acquire particles ranging from 38 to 74 μm for flotation tests. Besides, <5 μm samples were used for powder XRD and FTIR measurements. The samples of lepidolite (001) [6] and feldspar (010) [25] (most commonly exposed surfaces) were used for single-crystal XRD, contact angle, and AFM measurements. The chemical components and phase compositions of the mineral samples are provided in Table 1 and Fig. 1, respectively. The purity of lepidolite was 98%, while feldspar had a purity of 97%.

Table 1 Chemical compositions in samples of pure lepidolite and feldspar (wt.%)

Sample	Li_2O	F	Na_2O	Al_2O_3	SiO_2	K_2O	Fe_2O_3
Lepidolite	5.17	10.32	0.67	24.87	48.18	10.70	0.09
Feldspar	−	−	3.53	19.94	64.36	12.02	0.06

The activators used in this study were analytically pure calcium chloride ($CaCl_2$), magnesium chloride hexahydrate ($MgCl_2·6H_2O$), copper sulfate pentahydrate ($CuSO_4·5H_2O$), and lead nitrate ($Pb(NO_3)_2$). These substances can dissociate into Ca(II), Mg(II), Cu(II), and Pb(II),

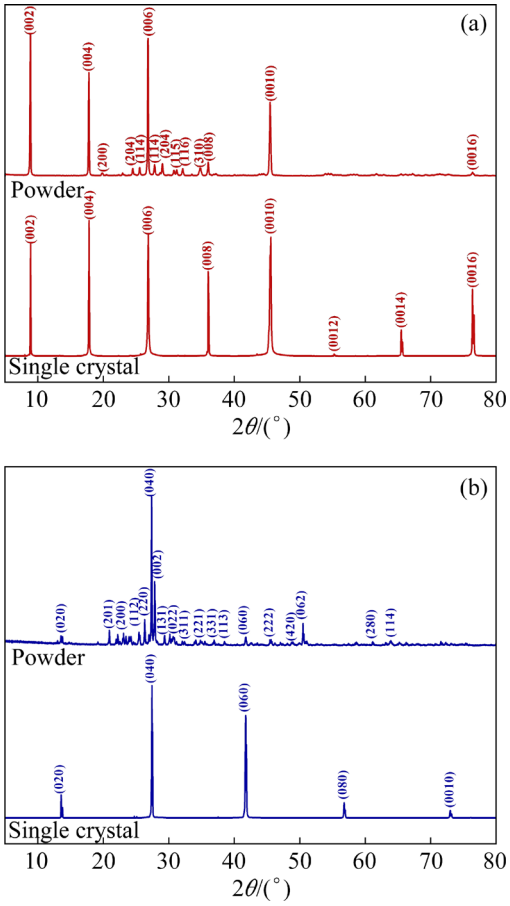

Fig. 1 Powder and single-crystal XRD patterns of lepidolite (a) and feldspar (b) samples

respectively. All these activators were derived from Shanghai Macklin Biochemical Technology Co., Ltd. (China). The collector SNOS ($C_{21}H_{38}NNaO_3$) was produced by saponification of analytically pure N-oleoylsarcosine ($C_{21}H_{39}NO_3$) and sodium hydroxide (NaOH) in a 1:1 molar ratio from Shanghai Macklin Biochemical Technology Co., Ltd. (China). The analytically pure sodium carbonate (Na_2CO_3) and hydrochloric acid (HCl) were purchased from Hunan Huihong Reagent Co., Ltd. (China), which were used as the regulators of pH. The deionized (DI) water was used for the preparation of reagent solutions and in the experimental procedure.

2.2 Micro-flotation tests

The micro-flotation tests were carried out on the hanging groove flotation machine of XFG type [26]. The sample mass of feed is 2 g in the flotation tests. The dual mixed minerals were composed of lepidolite and feldspar in a mass ratio of 1:1. The flowsheet of the micro-flotation test is depicted in Fig. 2. Moreover, the concentrates and tailings of single mineral flotation were filtrated, dried, and weighed to calculate the recovery of flotation by Eq. (1) precisely. Furthermore, the concentrates and tailings of dual mineral flotation were filtrated, dried, and weighed, then determined for Li_2O grades to calculate the Li_2O flotation recovery according to Eq. (2). All flotation tests were repeated at least three times, and the average deviations of the flotation results were calculated.

$$\varepsilon = \frac{m_1}{m_1 + m_2} \times 100\% \tag{1}$$

where ε (%) represents the recovery of single mineral flotation; m_1 (g) and m_2 (g) denote the masses of concentrate and tailing for the flotation tests, respectively.

$$\varepsilon_{Li_2O} = \frac{m_1 G_C}{m_1 G_C + m_2 G_T} \times 100\% \tag{2}$$

where ε_{Li_2O} (%) represents the Li_2O recovery in the concentrate of the dual mixed minerals flotation; G_C (%) and G_T (%) denote the Li_2O grades of concentrate and tailing, respectively.

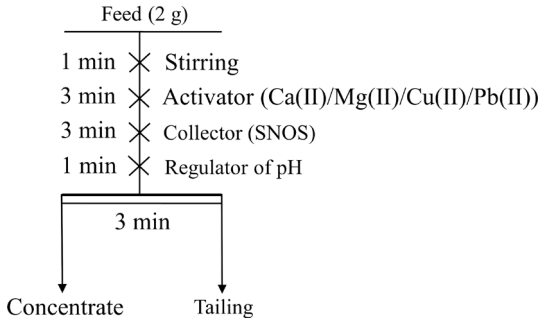

Fig. 2 Flowsheet of micro-flotation test

2.3 Contact angle measurements

The lepidolite and feldspar plates were placed in a beaker to measure the contact angle. Sequentially, DI water, activator, collector, and regulator were added. After immersing for 30 min, they were removed and dried using a stream of nitrogen. Then, they were placed horizontally on the measuring platform of the contact angle detector of the JY-82C type (Chengde Dingsheng Tester Co., Ltd., China) [27]. After that, a droplet of DI water was carefully placed on the mineral plates, and a clear image was captured using the provided software. Finally, the contact angle of the treated mineral plates was measured at least three times using the three-point method.

2.4 AFM measurements

The SNOS adsorption morphology on the surface of lepidolite (001) and feldspar (010) activated by the four metal ions was investigated using AFM (Multimode8, Bruker, USA) [28,29]. The same reagent treatment was applied to the mineral plates for contact angle and AFM measurements. The AFM measurements of the treated mineral plates were conducted using a single-crystal silicon probe (model SCANASYST-ATR). The scan frequency was adjusted to be 1 Hz, and the scan area was set to be 3.0 μm × 3.0 μm. Finally, the AFM images were flattened in the NanoScope Analysis software.

2.5 FTIR measurements

The measurements of FTIR were conducted on a transmission infrared spectrometer of IRAffinity-1 (Shimadzu, Japan) [30]. Firstly, 2 g of mineral powder was slowly placed in 100 mL conical flask. Subsequently, DI water, activator, collector, and regulator were added to form a suspension. Meanwhile, the suspension was stirred magnetically for 30 min. Next, the filtered samples were thoroughly dried in a 45 °C vacuum oven. Finally, the mineral powder was pressed, tested, and analyzed in sequence.

2.6 Species distribution calculations

The reaction and equilibrium constant of the reagent in a homogeneous system are shown in Table 2. The dissociation equilibrium constant (pK_a) of SNOS was measured using the potentiometric titrator (Metrohm, Switzerland) of 907 Titrando [31]. The cumulative stability constant (β) and solubility product constant (K_{sp}) of the four metal ions were obtained from Ref. [32]. The relationship between the concentration of different species produced by the reagent and the pH, in either a homogeneous or inhomogeneous system, could be calculated using the constants (β, K_{sp}, and pK_a) and reactions of the reagent.

2.7 DFT calculations

The primitive cells of lepidolite and feldspar were acquired from the American Mineralogist Crystal Structure Database. The DFT calculations were performed using the Cambridge Series Total Energy Package (CASTEP) [29,33]. The structures of SNOS, four metals, lepidolite, and feldspar were initially optimized, and their optimized geometries are presented in Fig. 3. Additionally, the water molecules were included in the simulation to mimic the aqueous environment. In the calculations, the Perdew−Burke−Ernzerh (PBE) functional was used to approximate the generalized gradient approximation (GGA) of the exchange-correlation potential. The convergence tolerance for the self-consistent field was 2.0×10^{-6} eV/atom. In the structural relaxation and energy calculations, the convergence criteria for energy, maximum force, maximum stress, and maximum displacement were 1.0×10^{-5} eV/atom, 0.03 eV/Å, 0.05 GPa, and 0.001 Å, respectively. The intermediate *k*-point grid and plane-wave cutoff energies for lepidolite were set at 6×6×1 and 780 eV, respectively. Similarly, for feldspar, the intermediate *k*-point lattice and plane-wave cutoff energies were set at 2×1×2 and 750 eV, respectively. The parameters of optimized lattice (*a*, *b*, *c*) for lepidolite were determined to be 5.198, 5.198, and 30.324 Å, which were found to be consistent with the experimental values (*a*=5.200 Å,

Table 2 Reaction and equilibrium constant of reagent

Reagent	Reaction	lg β	lg K_{sp}	pK_a
SNOS	$C_{21}H_{39}NO_3(l) \rightleftharpoons C_{21}H_{38}NO_3^- + H^+$	–	–	6.89
Ca(II)	$Ca(II)+OH^- \rightleftharpoons CaOH(I)$	1.4	−5.22	–
	$Ca(II)+2OH^- \rightleftharpoons Ca(OH)_2(aq)$	2.8		
Mg(II)	$Mg(II)+OH^- \rightleftharpoons MgOH(I)$	2.58	−11.15	–
	$Mg(II)+2OH^- \rightleftharpoons Mg(OH)_2(aq)$	1.0		
Cu(II)	$Cu(II)+OH^- \rightleftharpoons CuOH(I)$	6.3	−19.32	–
	$Cu(II)+2OH^- \rightleftharpoons Cu(OH)_2(aq)$	12.8		
	$Cu(II)+3OH^- \rightleftharpoons Cu(OH)_3^-$	14.5		
	$Cu(II)+4OH^- \rightleftharpoons Cu(OH)_4^{2-}$	16.4		
Pb(II)	$Pb(II)+OH^- \rightleftharpoons PbOH(I)$	6.3	−15.2	–
	$Pb(II)+2OH^- \rightleftharpoons Pb(OH)_2(aq)$	10.9		
	$Pb(II)+3OH^- \rightleftharpoons Pb(OH)_3^-$	13.9		

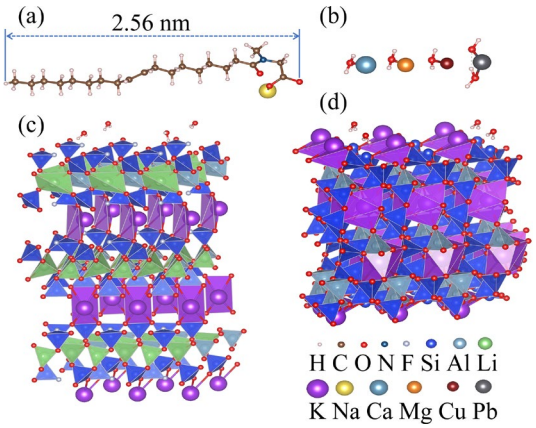

Fig. 3 Optimized geometries of SNOS (a), Ca(II)·H_2O/Mg(II)·H_2O/Cu(II)·H_2O/PbOH(I)·H_2O (b), surface of three-layer hydrated lepidolite (001) (c) and surface of three-layer hydrated feldspar (010) (d)

b=5.200 Å, and *c*=29.760 Å). Similarly, for feldspar, the optimized lattice parameters (*a*, *b*, *c*) were determined to be 8.541, 13.065, and 7.165 Å, which were also found to be consistent with the experimental values (*a*=8.588 Å, *b*=13.005 Å, and *c*=7.192 Å). The calculated values of the lattice parameters of lepidolite and feldspar closely matched the experimental values, suggesting that the method and parameter settings used in the calculation process were reasonable and reliable.

The optimized primitive cells of lepidolite and feldspar were cleaved along the (001) and (010) crystal planes, respectively, with the number of layers set to be 3 and the surface vectors set to be 3×2. Subsequently, vacuum slab crystals of lepidolite and feldspar with a vacuum thickness of 30 Å were constructed. The two-layer atoms at the bottom of the three-layer minerals were kept fixed in the geometry optimization and adsorption energy calculations. The adsorption energy 1 (E_{ads1}) of metal ions on the surface of lepidolite is calculated by Eq. (3). The adsorption energy 2 (E_{ads2}) of SNOS on the surface of Ca(II) activated lepidolite and feldspar is calculated by Eq. (4):

$$E_{ads1}=E_{system1}-(E_{metal\ ions}+E_{surface+water}) \quad (3)$$

where $E_{system1}$ is the energy of the optimized system with water, metal ions, and lepidolite (001) surface; $E_{metal\ ions}$ and $E_{surface+water}$ denote the energies of the metal ions and the lepidolite (001) surface with water, respectively.

$$E_{ads2}=E_{system2}-(E_{SNOS}+E_{surface+Ca+water}) \quad (4)$$

where $E_{system2}$ represents the energy of the optimized system with water, SNOS, metal ions, and mineral surface; E_{SNOS} and $E_{surface+Ca+water}$ denote the energies of SNOS and the mineral surface activated by Ca(II) in water, respectively.

3 Results and discussion

3.1 Micro-flotation tests results

To explore the influence of pulp pH on the recovery of lepidolite and feldspar using Ca(II), Mg(II), Cu(II), and Pb(II) as activators, micro-flotation tests of the single mineral were conducted at a concentration of 0.2 mmol/L SNOS, which are shown in Fig. 4. As shown in Figs. 4(a, b), using Ca(II) and Mg(II) as activators, the recoveries of lepidolite increased and then decreased with increasing pH, while the recovery of feldspar was less than 10%. Furthermore, at pulp pH of 7, the recoveries of lepidolite using Ca(II) and Mg(II) as activators were 94.7% and 93.4%, while the recoveries of feldspar were 3.9% and 5.7%, respectively. The results indicate that Ca(II) and Mg(II) selectively activate lepidolite while no not affect feldspar, leading to an increased difference in recovery between lepidolite and feldspar. In Figs. 4(c, d), it can be observed that the recoveries of lepidolite and feldspar increased and then decreased with an increased pH value when Cu(II) and Pb(II) were used as activators. Additionally, only at pH 5 using Cu(II) and pH 9.5 using Pb(II), the largest differences in flotation recovery between lepidolite and feldspar were 77.0% and 68.7%, respectively. The results show that Cu(II) and Pb(II) can activate both minerals, leading to a reduced difference in recovery. Therefore, the introduction of Ca(II) and Mg(II) in the flotation recovery of real lepidolite ores is considered appropriate. However, it is advisable to refrain from using Cu(II) and Pb(II) in the flotation recovery process of real lepidolite ores.

The influence of the concentration of activators (Ca(II), Mg(II), Cu(II), and Pb(II)) on the flotation behavior of lepidolite and feldspar is shown in Fig. 5. Figures 5(a, b) show that increasing the concentrations of Ca(II) and Mg(II) from 0.05 to 0.4 mmol/L resulted in a rapid increase in lepidolite recoveries, which then reached a plateau. On the other hand, feldspar recoveries remained below 10%. At a concentration of Cu(II) of

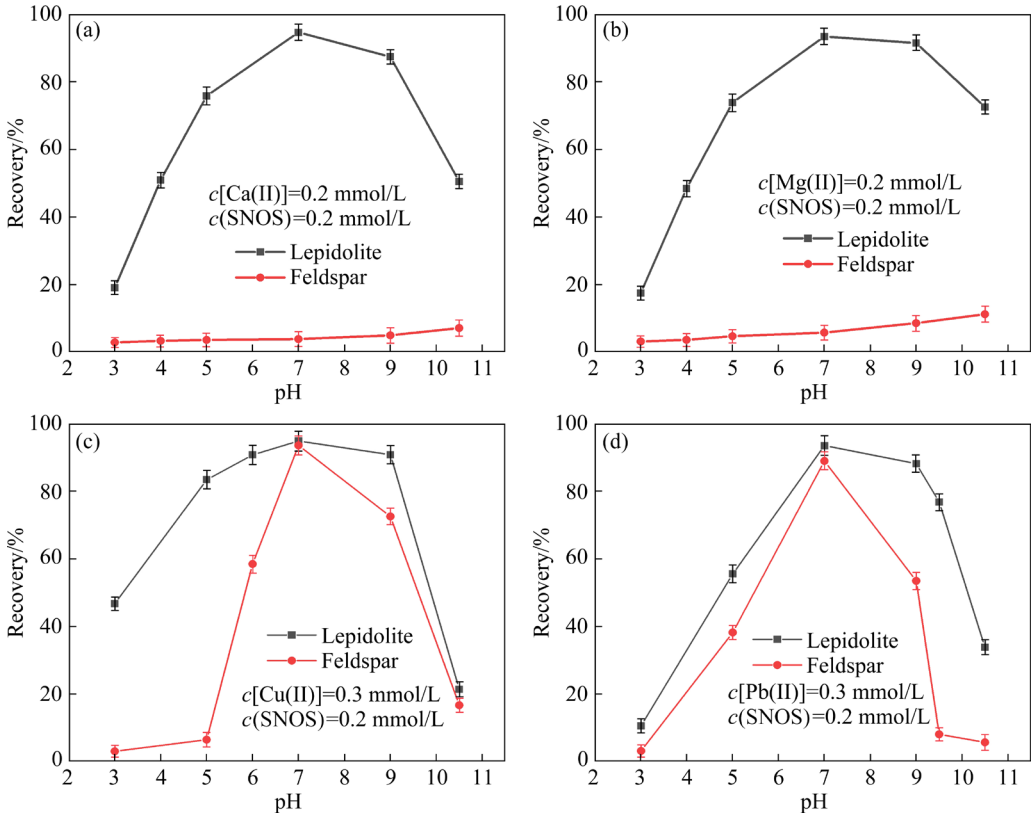

Fig. 4 Effects of pH on flotation recoveries of lepidolite and feldspar with Ca(II) (a), Mg(II) (b), Cu(II) (c), and Pb(II) (d) as activators (c(SNOS)=0.2 mmol/L)

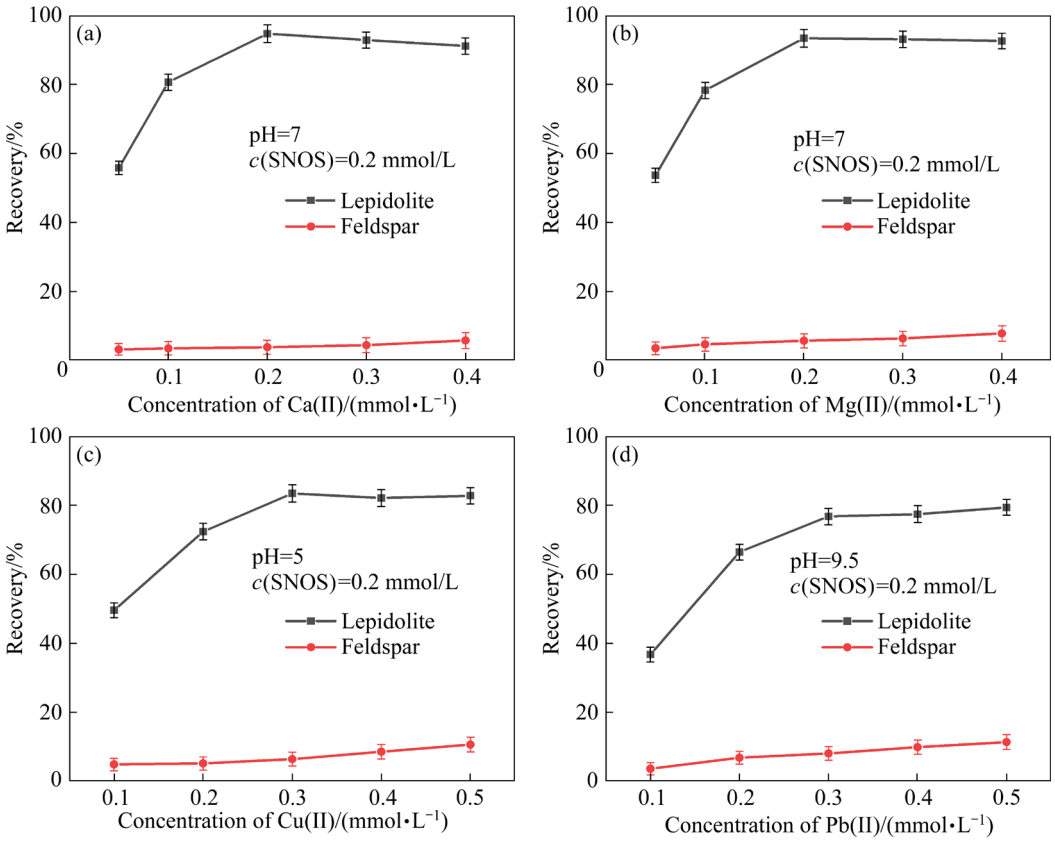

Fig. 5 Effect of metal ion concentration on flotation recoveries of lepidolite and feldspar with different metal ions as activators: (a) Ca(II); (b) Mg(II); (c) Cu(II); (d) Pb(II)

0.2 mmol/L, the largest difference in recovery between lepidolite and feldspar was 90.8%, while at 0.2 mmol/L Mg(II), the largest difference was 87.6%. When the recoveries of lepidolite increased and remained unchanged as the concentrations of Cu(II) and Pb(II) increased from 0.1 to 0.5 mmol/L, the recoveries of feldspar showed a gradual increase, as shown in Figs. 5(c, d). Moreover, at a concentration of 0.3 mmol/L metal ions, the recoveries of lepidolite using Cu(II) and Pb(II) were 83.4% and 76.7%, while the recoveries of feldspar were 6.4% and 8.0%, respectively. Consequently, Cu(II) and Pb(II) are less selective than Ca(II) and Mg(II) as activators for lepidolite under optimal conditions.

The effect of SNOS concentration on the recoveries of lepidolite and feldspar with Ca(II), Mg(II), Cu(II), and Pb(II) as activators is shown in Fig. 6. In Figs. 6(a, b), at *c*(SNOS) of 0.2 mmol/L, it is evident that the recovery differences between lepidolite and feldspar with Ca(II) and Mg(II) as activators were 90.8% and 87.6%, respectively. Meanwhile, it can be seen from Figs. 6(c, d) that the differences in flotation recovery between lepidolite and feldspar using Cu(II) and Pb(II) as activators were 77.0% and 68.7% at *c*(SNOS) of 0.2 mmol/L, respectively. The results demonstrate that SNOS has a strong collecting ability, which makes it a potential collector for the flotation separation of lepidolite and feldspar when the four mentioned metal ions are used as activators.

The flotation tests of dual mixed minerals were conducted to further verify the synergistic interaction of four metal ions separately and SNOS. According to Fig. 7, the use of Ca(II) as the activator resulted in a Li_2O recovery of 90.37% and a grade of 5.06% (Li_2O grade in pure lepidolite was 5.17%, as shown in Table 1) in the mixed mineral flotation concentrate. Using Mg(II) as the activator attained a concentrate with a higher Li_2O recovery of 91.10% and a lower Li_2O grade of 4.83%. When Cu(II) was used as the activator, the concentrate had the lowest Li_2O recovery of 87.57% and Li_2O grade of 4.56%. Similarly, when Pb(II) was employed, the concentrate achieved Li_2O recovery of 88.37% and the lowest Li_2O grade of 4.09%. Thus, the results

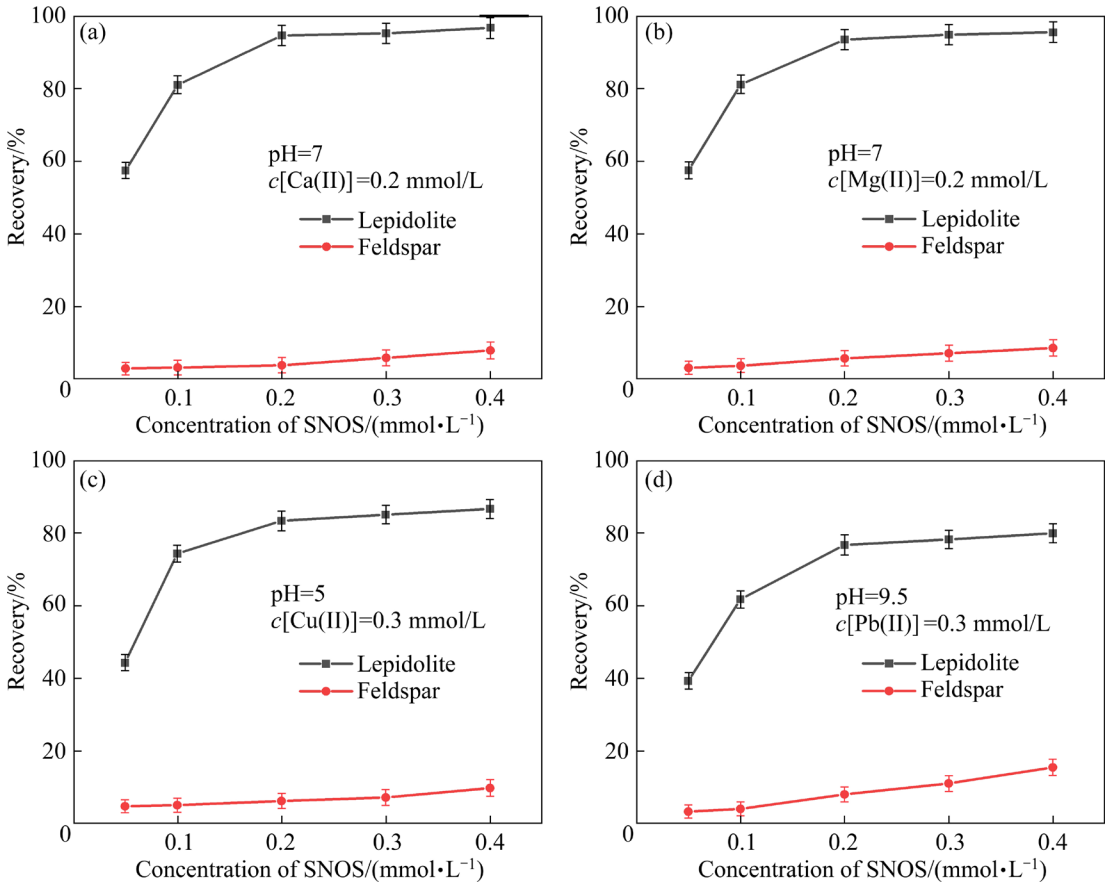

Fig. 6 Effect of SNOS concentration on flotation recoveries of lepidolite and feldspar with different metal ions as activators: (a) Ca(II); (b) Mg(II); (c) Cu(II); (d) Pb(II)

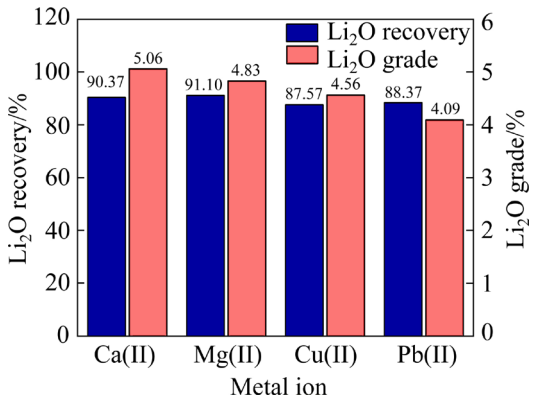

Fig. 7 Results of flotation tests of dual mixed minerals (pH=7, *c*[Ca(II)]=0.2 mmol/L, and *c*(SNOS)=0.2 mmol/L; pH=7, *c*[Mg(II)]=0.2 mmol/L, and *c*(SNOS)=0.2 mmol/L; pH=5, *c*[Cu(II)]=0.3 mmol/L, and *c*(SNOS)=0.2 mmol/L; pH=9.5, *c*[Pb(II)]=0.3 mmol/L, and *c*(SNOS)=0.2 mmol/L)

suggest that the activation efficiency of different metal ions on lepidolite using SNOS as the collector is in the order of Ca(II) > Mg(II) > Cu(II) > Pb(II).

3.2 Contact angle analysis

The contact angle results on the surface of lepidolite (001) treated with different concentrations of SNOS are presented in Fig. 8. It can be seen that the contact angle of the clean lepidolite (001) surface was measured to be 4.57°, suggesting that lepidolite exhibits high hydrophilicity, consistent with previous findings [9]. It is observed in Fig. 8 that the contact angle of the lepidolite (001) surface activated by the four metal ions increased rapidly and then slowly as the concentration of SNOS increased from 0 to 0.3 mmol/L. As the concentration of SNOS was 0.3 mmol/L, the contact angles of the lepidolite (001) surface with Ca(II), Mg(II), Cu(II), and Pb(II) as activators were 90.01°, 86.11°, 81.55°, and 77.96°, respectively. The results indicate that the combination of SNOS and metal ions has a substantial impact on altering the surface wettability of lepidolite (001). This alteration ranges from hydrophilic to hydrophobic, which is consistent with the flotation results in Figs. 4−7. Therefore, the hydrophobicity of the lepidolite (001) surface activated by different metal ions, when SNOS is employed as a collector, follows a consistent pattern: Ca(II) > Mg(II) > Cu(II) > Pb(II).

The contact angle results on the surface of feldspar (010) treated with different concentrations of SNOS are shown in Fig. 9. As can be seen in Fig. 9, the contact angle of the feldspar (010) surface was 28.09°, which is consistent with that reported previously [34]. In Fig. 9, the overall increment of the contact angle on the surface of feldspar (010) was tiny as the concentration of SNOS increased from 0 to 0.3 mmol/L. As the concentration of SNOS was 0.3 mmol/L, the contact angles of the feldspar (010) surface using Ca(II), Mg(II), Pb(II), and Cu(II) as activators were 36.54°, 38.12°, 41.78°, and 48.59°, respectively. These results show that the hydrophilicity of feldspar activated by Ca(II) and Mg(II) remains unchanged with increasing SNOS concentration. However, the hydrophilicity of feldspar activated by Cu(II) and Pb(II) undergoes significant changes, which is consistent with the flotation results shown in Figs. 4−7. Thus, this confirms that the surface of treated feldspar (010) containing SNOS and Ca(II) or SNOS and Mg(II) is hydrophilic and thus does not cause flotation of the gangue feldspar.

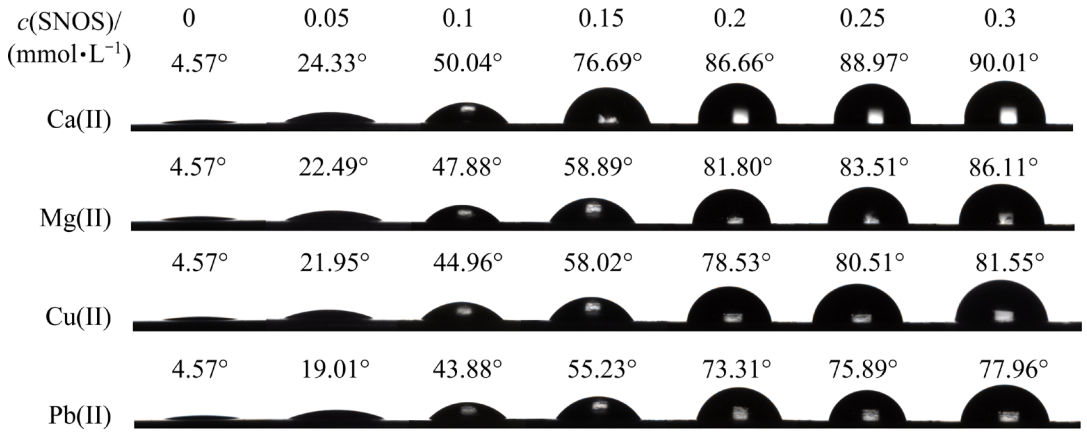

Fig. 8 Effect of different concentrations of SNOS on contact angles of lepidolite (001) surface (pH=7 and *c*[Ca(II)]= 0.2 mmol/L; pH=7 and *c*[Mg(II)]=0.2 mmol/L; pH=5 and *c*[Cu(II)]=0.3 mmol/L; pH=9.5 and *c*[Pb(II)]=0.3 mmol/L)

3.3 AFM imaging analysis

The AFM 3D images of the bare lepidolite (001) surface and the lepidolite (001) surface treated with SNOS and four metal ions are depicted in Fig. 10. The 3D image displayed that the bare lepidolite (001) surface was very smooth, with a tiny root mean square roughness (R_q) of 0.08 nm and a height difference of about 0.4 nm in the horizontal and vertical directions, as observed in Fig. 10(a). In Fig. 3(a), the theoretical length of the SNOS molecule is 2.56 nm. After SNOS and Ca(II) treatment, the lepidolite (001) surface became rough with R_q of 2.75 nm (Fig. 10(b)). This indicates that SNOS was adsorbed in multiple layers on the surface of Ca(II) activated lepidolite (001), with a significant adsorption height between 10 and 45 nm. The surface of SNOS and Mg(II) treated lepidolite (001) was also found to be rough in Fig. 10(c), with R_q of 0.55 nm and a primary adsorption height of SNOS of 2−13 nm. This

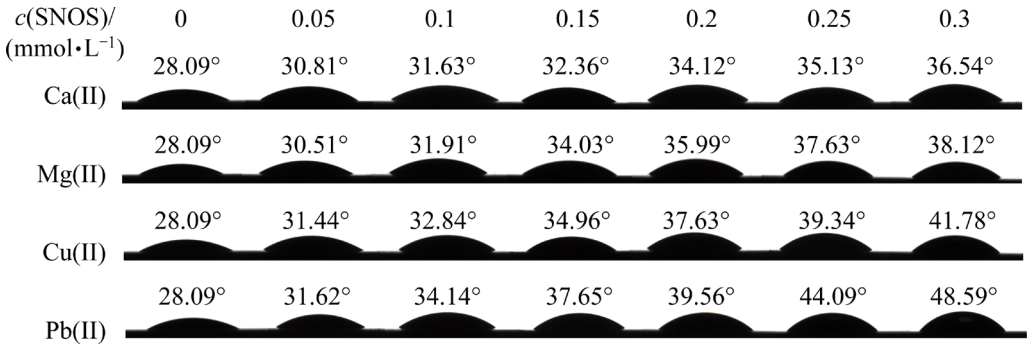

Fig. 9 Effect of different concentrations of SNOS on contact angles of feldspar (010) surface (pH=7 and c[Ca(II)]= 0.2 mmol/L; pH=7 and c[Mg(II)]=0.2 mmol/L; pH=5 and c[Cu(II)]=0.3 mmol/L; pH=9.5 and c[Pb(II)]=0.3 mmol/L)

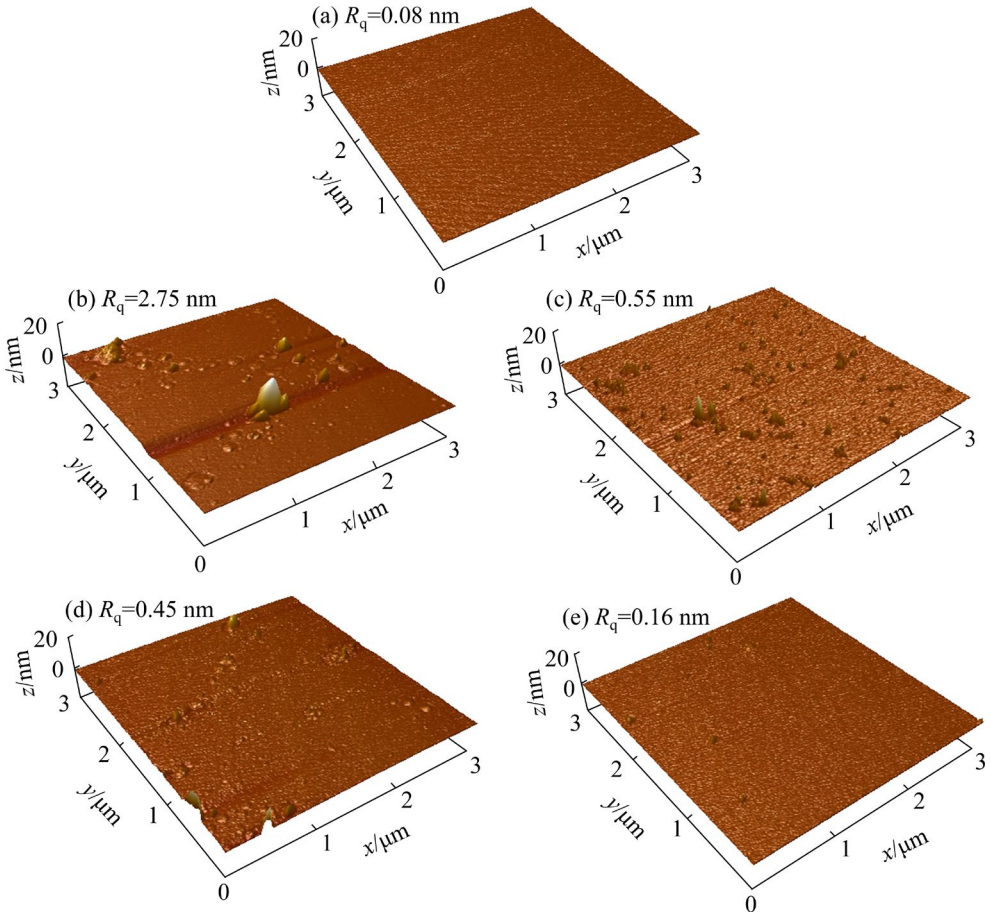

Fig. 10 AFM 3D images of bare lepidolite (001) surface (a) and lepidolite (001) surface after treatment with SNOS and different metal ions of Ca(II) (b), Mg(II) (c), Cu(II) (d), and Pb(II) (e)

indicates that SNOS can form both monolayer and multilayer adsorption on lepidolite. Similarly, in Fig. 11(d), the surface of SNOS and Cu(II) treated lepidolite was observed to be uneven, with R_q of 0.45 nm and mostly adsorption height of SNOS of 2−6 nm, demonstrating the occurrence of monolayer and bilayer adsorption of SNOS on lepidolite. In Fig. 10(e), the surface of SNOS and Pb(II) treated lepidolite was relatively flat, with R_q of 0.16 nm and most of the adsorption height of SNOS of 2−3 nm, suggesting the monolayer adsorption of SNOS on lepidolite. The results indicate that different metal ions influence the adsorption amount of SNOS on the lepidolite surface in the following order: Ca(II) > Mg(II) > Cu(II) > Pb(II).

Figure 11 displays the AFM 3D images for the bare feldspar (010) surface and the feldspar (010) surface after the treatment with SNOS and four metal ions. It can be seen in Fig. 11(a) that the bare feldspar (010) surface was very smooth with R_q of 0.12 nm. The 3D images in Figs. 11(b, c) show that the feldspar (010) surfaces using Ca(II) and Mg(II) were smooth, with R_q of 0.14 and 0.16 nm, respectively. Since their roughness remains relatively constant, it is difficult for SNOS to form stable adsorption on the surface of the Ca(II) or Mg(II) activated feldspar (010). In Fig. 11(d), the R_q of the feldspar (010) surface after Cu(II) and SNOS treatment increased to 0.28 nm, indicating that a small amount of SNOS was adsorbed on feldspar. Moreover, the 3D images in Fig. 11(e) depict that the surface of SNOS and Pb(II) treated feldspar (010) was not only rough but also had R_q of 0.60 nm, with the corresponding adsorption height of SNOS of 2−3 nm, suggesting the monolayer adsorption of SNOS on feldspar. A comparison of Figs. 10 and 11 reveal that the selective activation of lepidolite by Ca(II) and Mg(II) is significantly better than that of Cu(II) and Pb(II).

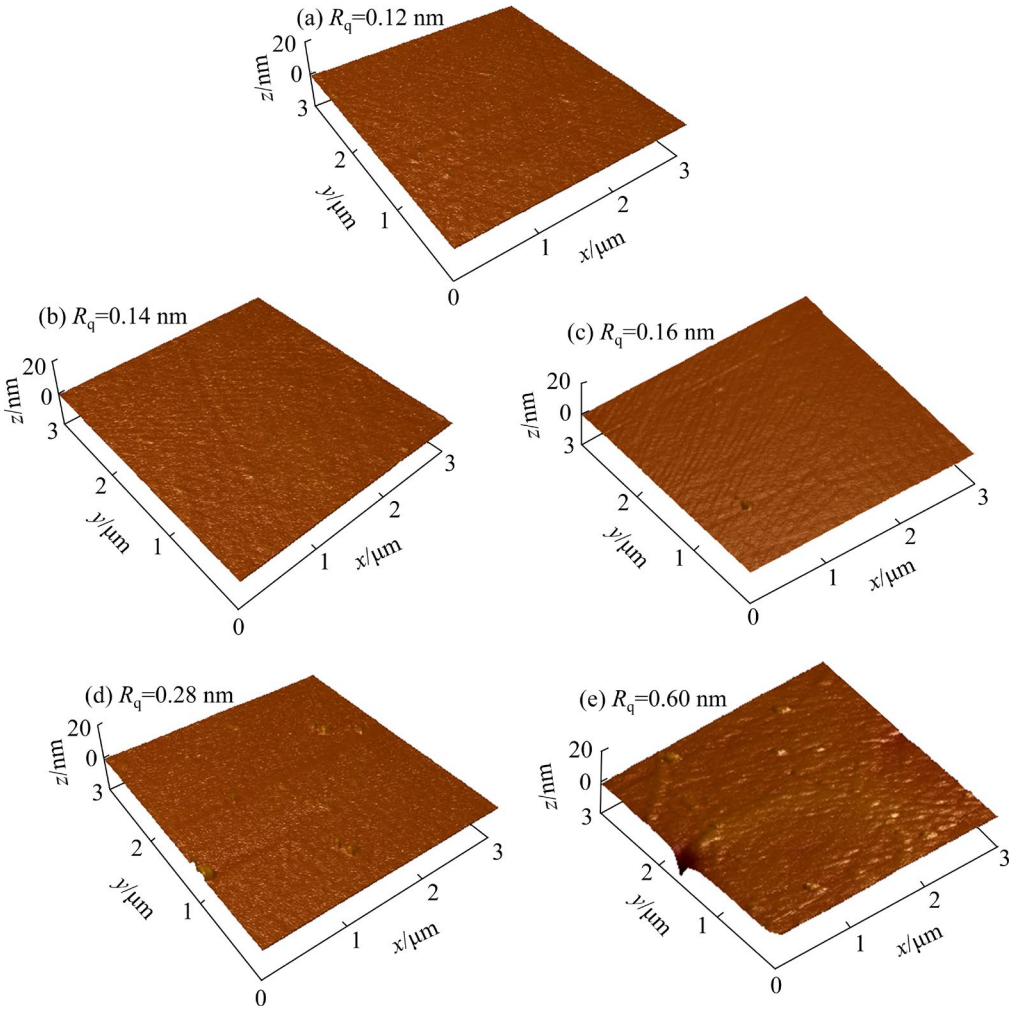

Fig. 11 AFM 3D images of bare feldspar (010) surface (a) and feldspar (010) surface after treatment with SNOS and different metal ions of Ca(II) (b), Mg(II) (c), Cu(II) (d), and Pb(II) (e)

3.4 FTIR spectra analysis

To better analyze the SNOS adsorption on the mineral surface activated by the four metal ions, FTIR spectra were performed on the lepidolite and feldspar in the presence and absence of the SNOS and four metal ions, as depicted in Fig. 12. The FTIR spectrum of SNOS is provided in Fig. 12(a), and the peaks at 2924 and 2854 cm^{-1} correspond to the stretching vibrations of —CH_2— and —CH_3 groups [21,22]. Specifically, the peak at 1607 cm^{-1} is caused by the asymmetric stretching vibration of the —CON— group [35,36]. At the same time, the peaks at 1562, 1460, and 1423 cm^{-1} are attributed to the stretching vibration of —COO— group [37].

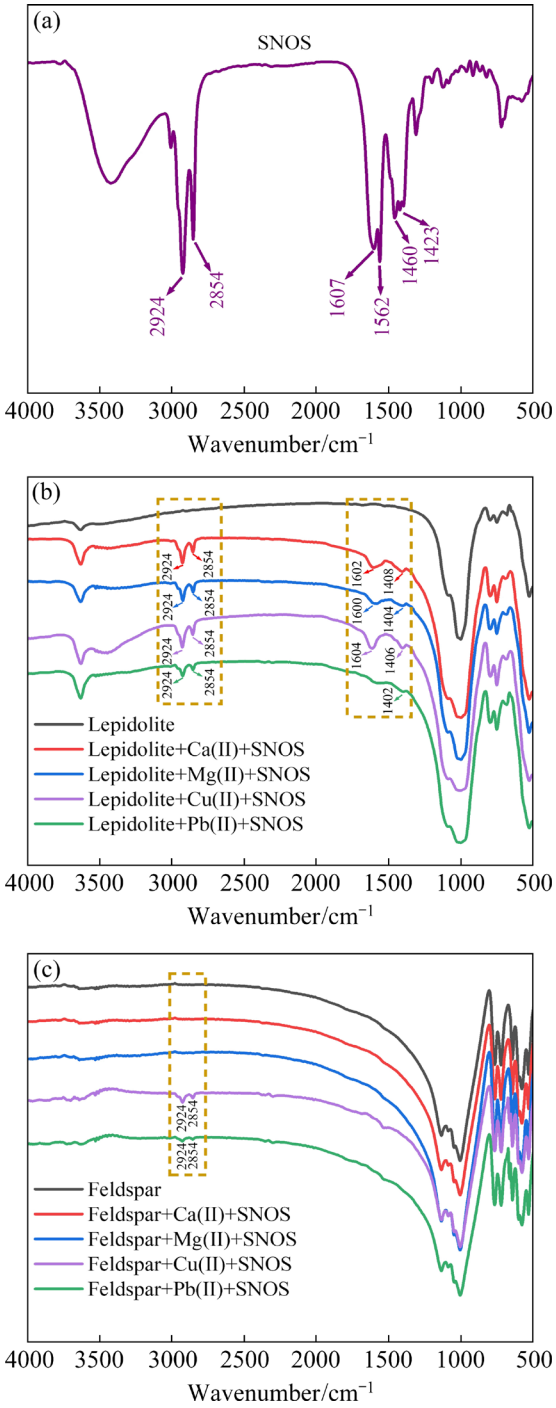

Fig. 12 FTIR spectra of SNOS (a), lepidolite in presence and absence of four metal ions and SNOS (b), and feldspar in presence and absence of four metal ions and SNOS (c)

In Fig. 12(b), strong peaks appeared at 2924 and 2854 cm^{-1} on the lepidolite surface after the treatment with Ca(II) and SNOS. Simultaneously, the other characteristic peaks belonged to the stretching vibration of —CON— and —COO— from SNOS, and were observed at 1602 and 1408 cm^{-1}, respectively. Additionally, new peaks appeared at 2924, 2854, 1600, and 1404 cm^{-1} on lepidolite surface after being treated with Mg(II) and SNOS, which were attributed to —CH_2—, —CH_3, —CON—, and —COO— groups, respectively. Moreover, these new peaks appeared equally at 2924 and 2854 cm^{-1} on the lepidolite treated with Cu(II) and SNOS or Pb(II) and SNOS. Therefore, after the interaction of SNOS with the four metal ions activated lepidolite, the peak of —COO— group on the lepidolite surface exhibited an obvious change compared with the original peak of —COO— group from SNOS, indicating the absence of strong chemical adsorption of SNOS on the four metal ions activated lepidolite.

In Fig. 12(c), there was no new peak in the FTIR spectra of the feldspar treated with Ca(II) and SNOS or Mg(II) and SNOS, indicating that SNOS had no chemisorption on the surface of feldspar activated by Ca(II) and Mg(II). In addition, these weak peaks were presented at 2926 and 2854 cm^{-1} on the feldspar surface treated with Ca(II) and SNOS or Mg(II) and SNOS, attributing to —CH_2— and —CH_3 stretching vibration of SNOS, indicating that SNOS exhibited the faint adsorption on the Cu(II) and Pb(II) activated feldspar surface. These results reveal that the activation effect of Ca(II) and Mg(II) on the feldspar was found to be weaker compared to Cu(II) and Pb(II). Therefore, using Ca(II) and Mg(II) as activators, along with SNOS as a collector, proved to be beneficial for the flotation separation of lepidolite and gangue feldspar.

3.5 Species distribution analysis

The influence of pH on the species distribution of the agents is widely recognized, requiring

solution-chemistry calculations for flotation [38]. In order to investigate the main active components of SNOS, $CaCl_2$, $MgCl_2·6H_2O$, $CuSO_4·5H_2O$, and $Pb(NO_3)_2$ under the optimal pH conditions, the species distribution is shown in Fig. 13. At pH 7, SNOS chiefly present in the form of monovalent anion $C_{21}H_{38}NO_3^-$ and liquid $C_{21}H_{39}NO_3$(l), as shown in Fig. 13(a). Furthermore, when the pH is 7, $CaCl_2$ exists mainly as Ca(II), with trace amounts of CaOH(I) and $CaOH_2$(aq), as shown in Fig. 13(b). Moreover, when pH=7, $MgCl_2·6H_2O$ is mainly in the form of Mg(II) with trace amounts of MgOH(I), as shown in Fig. 13(c). In addition, when the pH is equal to 7, $CuSO_4·5H_2O$ is mainly in the form of Cu(II) with small amounts of CuOH(I), $CuOH_2$(aq), $Cu(OH)_3^-$, and $Cu(OH)_4^{2-}$, as shown in Fig. 13(d). Finally, at pH=9.5, $Pb(NO_3)_2$ is primarily present as PbOH(I), $PbOH_2$(s), and $PbOH_2$(aq), with small

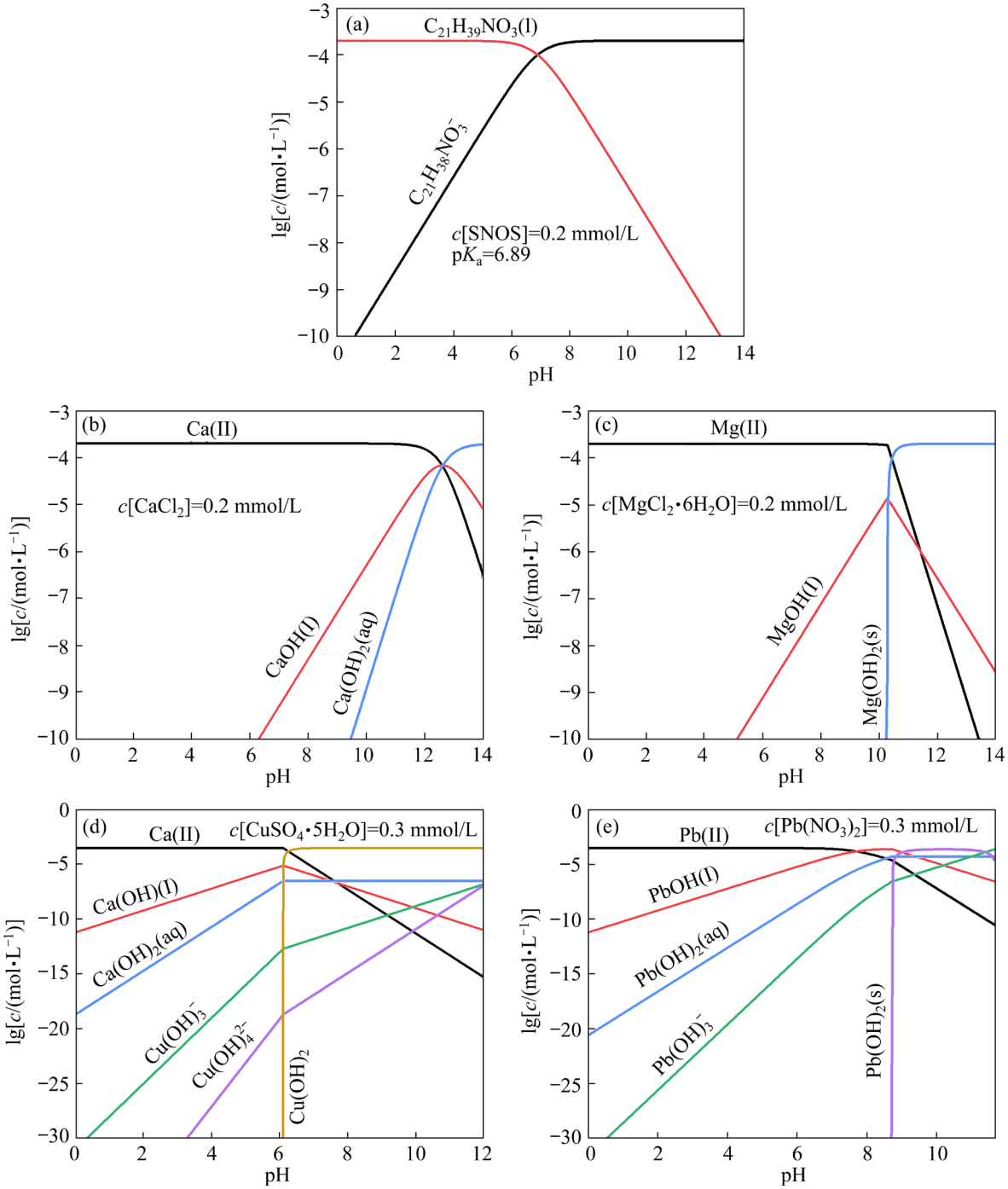

Fig. 13 Diagrams of species distribution for SNOS (a), $CaCl_2$ (b), $MgCl_2·6H_2O$ (c), $CuSO_4·5H_2O$ (d), and $Pb(NO_3)_2$ (e) at different pH

amounts of Pb(II) and $Pb(OH)_3^-$, as shown in Fig. 13(e). Therefore, under the optimal flotation conditions, SNOS, Ca(II), Mg(II), Cu(II), and $Pb(NO_3)_2$ in solution are primarily present as $C_{21}H_{38}NO_3^-$, Ca(II), Mg(II), Cu(II), and PbOH(I), respectively.

3.6 DFT calculation analysis

Based on the dominant components of each of the four metal ions in Fig. 13 and considering that all metal ions hydrate in solution, we identified Ca(II)·H_2O, Mg(II)·H_2O, Cu(II)·H_2O, and PbOH(I)·H_2O as adsorbates on the lepidolite (001) surface. To explore the adsorption models of the four metal ions on the lepidolite (001) surface, the DFT calculations were conducted, as shown in Fig. 14. Figures 14(a, b) show that Ca(II) and Mg(II) have similar adsorption models on lepidolite, binding well to the (001) surface. This is achieved by bonding F, O2, and O3 atoms in lepidolite with Ca or Mg atoms. The study found that in Fig. 14(c), Cu(II)·H_2O could bind more effectively to the lepidolite (001) surface due to the bonding of O2 and O3 atoms of lepidolite with the Cu atom. Similarly, in Fig. 14(d), PbOH(I)·H_2O was observed to bind to the lepidolite (001) surface due to the bonding of F and O2 atoms of lepidolite with the Cu atom. The above results showed that Ca(II)·H_2O and Mg(II)·H_2O had a higher tendency to interact with lepidolite compared to Cu(II)·H_2O and PbOH(I)·H_2O.

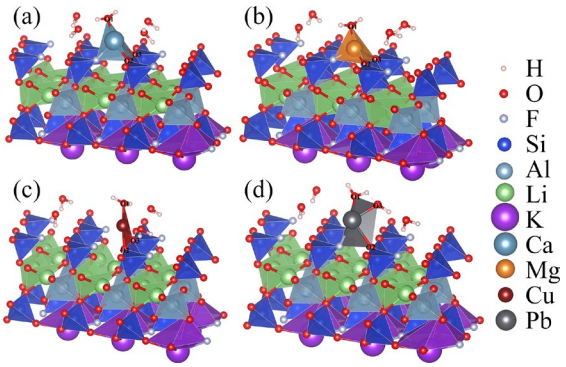

Fig. 14 Adsorption configuration of Ca(II)·H_2O (a), Mg(II)·H_2O (b), Cu(II)·H_2O (c), and PbOH(I)·H_2O (d) on one-layer lepidolite (001) surface

The interaction strength, bond lengths, and adsorption energy for adsorbates (Ca(II)·H_2O, Mg(II)·H_2O, Cu(II)·H_2O, and PbOH(I)·H_2O) on the lepidolite (001) surface were calculated in Table 2. The bond lengths between metals (Ca, Mg, Cu, and Pb) and oxygen (O) or fluorine (F) atoms were measured on lepidolite with different adsorbates. When Ca(II)·H_2O was adsorbed, the bond lengths of O1—Ca, O2—Ca, O3—Ca, and F—Ca were 2.371, 2.306, 2.265, and 2.101 Å, respectively. With Mg(II)·H_2O adsorption, the bond lengths of O1—Mg, O2—Mg, O3—Mg, and F—Mg were 2.017, 2.064, 1.993, and 1.843 Å, respectively. When Cu(II)·H_2O was adsorbed, the bond lengths of O1—Cu, O2—Cu, and O3—Cu were 1.901, 1.877, and 2.643 Å, respectively. Finally, with PbOH(I)·H_2O adsorption, the bond lengths of O1—Pb, O2—Pb, O3—Pb, and F—Pb were 2.532, 2.192, 2.506, and 2.655 Å, respectively. According to Table 2, the adsorption energy values for Ca(II)·H_2O, Mg(II)·H_2O, Cu(II)·H_2O, and PbOH(I)·H_2O on the lepidolite (001) surface were −923.45, −822.96, −574.66, and −395.50 kJ/mol, respectively. These results suggest that Ca(II)·H_2O exhibited a higher affinity for adsorption onto lepidolite than other hydrated metal ions based on its higher adsorption energy.

Table 2 Bond length and adsorption energy for Ca(II)·H_2O, Mg(II)·H_2O, Cu(II)·H_2O, and PbOH(I)·H_2O on lepidolite (001) surface

Adsorbate	Bond	Length/Å	E_{ads1}/(kJ·mol^{-1})
Ca(II)·H_2O	O1—Ca	2.371	−923.45
	O2—Ca	2.306	
	O3—Ca	2.265	
	F—Ca	2.101	
Mg(II)·H_2O	O1—Ca	2.017	−822.96
	O2—Ca	2.064	
	O3—Ca	1.993	
	F—Ca	1.843	
Cu(II)·H_2O	O1—Ca	1.901	−574.66
	O2—Ca	1.877	
	O3—Ca	2.643	
PbOH(I)·H_2O	O1—Ca	2.532	−395.50
	O2—Ca	2.192	
	O3—Ca	2.506	
	F—Ca	2.655	

The adsorption models of SNOS on the lepidolite (001) and feldspar (010) surfaces were calculated to explore their bonding forms thoroughly. As seen in Fig. 15, SNOS could bind to the adsorbate (Ca(II)·H_2O) on the surface of lepidolite (001) and feldspar (010), respectively, which was obtained through the bonding of O1, O2 and O3 atoms of SNOS to Ca atom of the adsorbate. By comparing Figs. 15(a, b), Ca(II)·H_2O could bind to O5, O6, and F atoms of lepidolite, while only bound to O5 of feldspar. This difference in binding resulted in a significant contrast between the two adsorption models. Additionally, the surface of lepidolite (001) contained more O and F atoms than the surface of feldspar (010). These findings suggest that lepidolite exhibited a more pronounced activation in the presence of Ca(II).

The bond lengths and adsorption energy for SNOS on the lepidolite (001) and feldspar (010) surfaces are summarized in Table 3. When SNOS was adsorbed on Ca(II) activated lepidolite, the bond lengths of O1—Ca, O2—Ca, O3—Ca, O4—Ca, O5—Ca, O6—Ca, and F—Ca were 2.386, 2.531, 2.370, 2.427, 2.349, 2.587, and 2.409 Å, respectively. With the adsorption of SNOS on feldspar, the bond lengths of O1—Ca, O2—Ca, O3—Ca, O4—Ca, and O5—Ca were 2.596, 2.333, 2.313, 2.394, and 2.142 Å, respectively. Table 3 demonstrates that the adsorption energy of SNOS on the Ca(II)-activated lepidolite (001) surface was −1248.91 kJ/mol, significantly lower than that of Ca(II)-activated feldspar (010) (−598.84 kJ/mol). This indicates that SNOS was more prone to be adsorbed on Ca(II)-activated lepidolite.

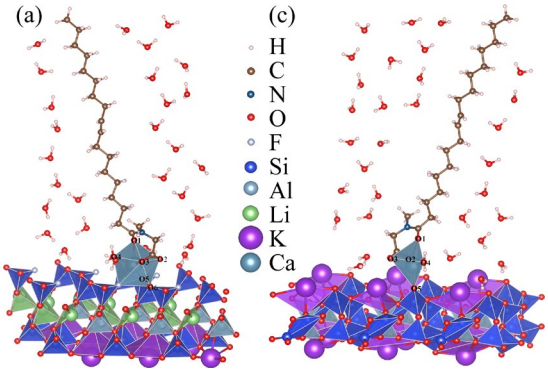

Fig. 15 Adsorption configurations of SNOS on one-layer lepidolite (001) surface (a) and feldspar (010) surface (b) activated by Ca(II)

Table 3 Bond length and adsorption energy for SNOS onto Ca(II) activated lepidolite (001) and feldspar (010) surface

Ca(II) activated mineral surface	Bond	Length/Å	E_{ads2}/(kJ·mol^{-1})
Lepidolite (001) + Ca(II)·H_2O	O1—Ca	2.386	−1248.91
	O2—Ca	2.531	
	O3—Ca	2.370	
	O4—Ca	2.427	
	O5—Ca	2.349	
	O6—Ca	2.587	
	F—Ca	2.409	
Feldspar (010) + Ca(II)·H_2O	O1—Ca	2.596	−598.84
	O2—Ca	2.333	
	O3—Ca	2.313	
	O4—Ca	2.394	
	O5—Ca	2.142	

4 Conclusions

(1) The flotation experiments of binary mixed minerals were conducted using Ca(II), Mg(II), Cu(II), and Pb(II) as activators and SNOS as a collector. The concentrates had Li_2O recoveries of 90.37%, 91.10%, 87.57%, and 88.37%, with Li_2O grades of 5.06%, 4.83%, 4.56%, and 4.09%, respectively. The results indicated that Ca(II) and Mg(II) were more selective activators.

(2) The contact angle, AFM, and FTIR analysis revealed that the surface of Ca(II)-activated lepidolite became more hydrophobic and rougher when SNOS were added, attributed to the multilayer adsorption of SNOS. In contrast, the surface of Ca(II)-activated feldspar remained hydrophilic and flat as there was minimal adsorption of SNOS.

(3) The species distribution and DFT calculations verified that SNOS showed a stronger tendency to be adsorbed on Ca(II)-activated lepidolite compared to feldspar. These findings suggested using Ca(II) as activator and SNOS as a collector is a promising reagent scheme for the efficient recovery of lithium from aluminosilicate ore.

CRediT authorship contribution statement

Guo-yuan XIANG: Methodology, Data curation,

Investigation, Formal analysis, Visualization, Writing − Original draft; **Rui-hua FAN:** Methodology, Investigation, Visualization; **Wen-tao ZHU:** Methodology, Data curation, Investigation; **Wei SUN:** Conceptualization, Methodology, Supervision; **Ren-ji ZHENG** and **Zhi-yong GAO:** Conceptualization, Methodology, Supervision, Writing − Review & editing, Funding acquisition.

Declaration of competing interest

The authors declare that they have no known competing financial interests or personal relationships that could have appeared to influence the work reported in this paper.

Acknowledgments

The authors acknowledge financial support from the National Natural Science Foundation of China (Nos. U2067201, 52204300), the National 111 Project, China (No. B14034), the Fundamental Research Funds for the Central Universities of Central South University, China (No. 2021zzts0297). This work was partly carried out in the High-Performance Computing Centers of Central South University.

References

[1] ABDULLAEV R N, KHAIRULIN R A, KOZLOVSKII Y M, AGAZHANOV A S, STANKUS S V. Density of magnesium and magnesium-lithium alloys in solid and liquid states [J]. Transactions of Nonferrous Metals Society of China, 2019, 29(3): 507−514.

[2] MARTIN G, RENTSCH L, HÖCK M, BERTAU M. Lithium market research-global supply, future demand and price development [J]. Energy Storage Materials, 2017, 6: 171−179.

[3] AMBROSE H, KENDALL A. Understanding the future of lithium. Part 1: Resource model [J]. Journal of Industrial Ecology, 2020, 24(1): 80−89.

[4] SWAIN B. Recovery and recycling of lithium: A review [J]. Separation and Purification Technology, 2017, 172: 388−403.

[5] HUANG Zhi-qiang, SHUAI Shu-yi, WANG Hong-ling, LIU Ru-kuan, ZHANG Shi-yong, CHENG Chen, HU Ya-jing, YU Xin-yang, HE Gui-chun, FU Weng. Froth flotation separation of lepidolite ore using a new Gemini surfactant as the flotation collector [J]. Separation and Purification Technology, 2022, 282: 119122.

[6] KORBEL C, FILIPPOVA I V, FILIPPOV L O. Froth flotation of lithium micas — A review [J]. Minerals Engineering, 2023, 192: 107986.

[7] LIU Zi-yu, JIAO Fen, QIN Wen-qing, WEI Qian. Collision–attachment law of lepidolite, feldspar and quartz with bubbles in the combined cationic and anionic collector system [J]. Physicochemical Problems of Mineral Processing, 2022: 58: 252861384.

[8] BAI Yang, CUI Wan-shun, GAO Yu-juan, WEN Wei-xiang, SUN Yi-kun, YAN Ping-ke. Synergistic mechanism of mixed cationic/anionic collectors on lepidolite flotation from the perspective of improving the performance of flotation foam [J]. Colloids and Surfaces A: Physicochemical and Engineering Aspects, 2023, 656: 130354.

[9] HUANG Zhi-qiang, LI Wen-yuan, HE Gui-chun, SHEN Lou-yan, CHEN Xiao-ai, SHUAI Shu-yi, LI Fang-xu, WANG Hong-ling, LIU Ru-kuan, ZHANG Shi-yong, CHENG Chen, OUYANG Liao-yuan, YU Xin-yang, FU Weng. Adsorption mechanism of amidoxime collector on the flotation of lepidolite: Experiment and DFT calculation [J]. Langmuir, 2022, 38(50): 15858−15865.

[10] HUANG Zhi-qiang, ZHANG Shi-yong, CHENG Chen, WANG Hong-ling, LIU Ru-kuan, HU Ya-jing, HE Gui-chun, YU Xin-yang, FU Weng. Recycling lepidolite from tantalum–niobium mine tailings by a combined magnetic–flotation process using a novel Gemini surfactant: From tailings dams to the “bling” raw material of lithium [J]. ACS Sustainable Chemistry & Engineering, 2020, 8(49): 18206−18214.

[11] CHOI J, KIM W, CHAE W, KIM S B, KIM H. Electrostatically controlled enrichment of lepidolite via flotation [J]. Materials Transactions, 2012, 53(12): 2191−2194.

[12] WEI Qian, FENG Li-qin, DONG Liu-yang, JIAO Fen, QIN Wen-qing. Selective co-adsorption mechanism of a new mixed collector on the flotation separation of lepidolite from quartz [J]. Colloids and Surfaces A: Physicochemical and Engineering Aspects, 2021, 612: 125973.

[13] SOUSA R, RAMOS V, GUEDES A, DE SOUSA A B, NORONHA F, LEITE M M. Flotation of lithium ores to obtain high-grade Li_2O concentrates. Are there any mineralogical limitations? [J]. International Journal of Mining, Materials, and Metallurgical Engineering, 2019, 5(1): 7−18.

[14] JIA Mu-xin, SUN Chuan-yao. Study on adsorption behavior of metal ions on some silicate minerals [J]. Mining & Metallurgy, 2001, 10(3): 25−30.

[15] XIE Rui-qi, ZHU Yi-min, LIU Jie, LI Yan-jun. Effects of metal ions on the flotation separation of spodumene from feldspar and quartz [J]. Minerals Engineering, 2021, 168: 106931.

[16] SUN Ning, WANG Guo-dong, GE Peng, SUN Wei, XU Long-hua, Tang Hong-hu, WANG Li. Selective flotation of quartz from feldspar using hydroxypropyl starch as depressant [J]. Minerals Engineering, 2023, 195: 108022.

[17] SUN Wen-juan, HAN Hai-sheng, SUN Wei, WANG Ruo-lin, WEI Zhao. Novel insights into the role of colloidal calcium dioleate in the flotation of calcium minerals [J]. Minerals Engineering, 2022, 175: 107274.

[18] HE Jian-yong, SUN Wei, ZENG Hong-bo, FAN Rui-hua, HU Wen-jihao, GAO Zhi-yong. Unraveling roles of lead ions

in selective flotation of scheelite and fluorite from atomic force microscopy and first-principles calculations [J]. Minerals Engineering, 2022, 179: 107424.

[19] TIAN Meng-jie, GAO Zhi-yong, SUN Wei, HAN Hai-sheng, SUN Lei, HU Yue-hua. Activation role of lead ions in benzohydroxamic acid flotation of oxide minerals: New perspective and new practice [J]. Journal of Colloid and Interface Science, 2018, 529: 150−160.

[20] WANG Ruo-lin, ZHANG Hong-liang, SUN Wen-juan, HAN Hai-sheng. The inhibiting effect of Pb-starch on chlorite flotation and its adsorption configuration based on DFT computation [J]. Applied Surface Science, 2023, 610: 155482.

[21] GAO Zhi-yong, JIANG Zhe-yi, SUN Wei, POOLEY S G, WANG Jian-jun, LIU Yun-feng, XU Feng-ping, WANG Qing-hong, ZENG Lin, WU Yuan-chan. New role of the conventional foamer sodium N-lauroylsarcosinate as a selective collector for the separation of calcium minerals [J]. Journal of Molecular Liquids, 2020, 318: 114031.

[22] MIAO Ze-kun, TAO Li-ming, WANG Jian-jun, JIANG Zhe-yi, PENG Tao, SUN Wei, GAO Zhi-yong. Selective separation of fluorite from scheelite using N-decanoylsarcosine sodium as a novel collector [J]. Minerals, 2022, 12(7): 855.

[23] GAO Zhi-yong, JIANG Zhe-yi, SUN Wei, GAO Yue-sheng. Typical roles of metal ions in mineral flotation: A review [J]. Transactions of Nonferrous Metals Society of China, 2021, 31(7): 2081−2101.

[24] WANG Xing-jie, ZHANG Yi-min, LIU Tao, CAI Zhen-lei. Influence of metal ions on muscovite and calcite flotation: With respect to the pre-treatment of vanadium bearing stone coal [J]. Colloids and Surfaces A: Physicochemical and Engineering Aspects, 2019, 564: 89−94.

[25] XU Long-hua, PENG Tie-feng, TIAN Jia, LU Zhong-yuan, HU Yue-hua, SUN Wei. Anisotropic surface physicochemical properties of spodumene and albite crystals: Implications for flotation separation [J]. Applied Surface Science, 2017, 426: 1005−1022.

[26] WEI Qian, DONG Liu-yang, YANG Cong-ren, LIU Xue-duan, JIAO Fen, QIN Wen-qing. Selective depression mechanism of combination of lime and sodium humate on arsenopyrite in flotation separation of Zn−As bulk concentrate [J]. Transactions of Nonferrous Metals Society of China, 2022, 32(2): 668−681.

[27] DONG Liu-yang, WEI Qian, QIN Wen-qing, JIAO Fen. Selective adsorption of sodium polyacrylate on calcite surface: Implications for flotation separation of apatite from calcite [J]. Separation and Purification Technology, 2020, 241: 116415.

[28] PAN Zu-chao, ZHANG Yi-sheng, HU Jun-jie, JIAO Fen, QIN Wen-qing. Camphor leaf extract as neoteric and environmentally friendly depressant in flotation separation of scheelite and calcite [J]. Transactions of Nonferrous Metals Society of China, 2023, 33(1): 275−284.

[29] TAO Li-ming, SUN Wei, WANG Jian-jun. Selective separation of fluorite from calcite using saponified tridecanoic acid as a novel collector [J]. Mineral Processing and Extractive Metallurgy Review, 2024, 45: 509−521.

[30] WANG Cong, REN Shuai, SUN Wei, WU Si-hui, TAO Li-ming, DUAN Yao, WANG Jian-jun, GAO Zhi-yong. Selective flotation of scheelite from calcite using a novel self-assembled collector [J]. Minerals Engineering, 2021, 171: 107120.

[31] GAO Ya, FU Xin-zhuang, PAN Zu-jiang, YUE Tong, SUN Wei. Surface complexation model theory application in NaOL and CTAB collector adsorption differences of diaspore and kaolinite flotation [J]. Separation and Purification Technology, 2022, 295: 121288.

[32] WANG Dian-zuo, HU Yue-hua. Solution chemistry of flotation [M]. Changsha: Hunan Science & Technology Press, 1988.

[33] ZHANG Wan-jia, WU Yun-xia, FAN Rui-hua, CAO Jian, POOLEY S, SUN Wei, GAO Zhi-yong. Improved flotation separation of sulfide minerals by synthesized surfactant based on para-position methyl effect [J]. Separation and Purification Technology, 2022, 297: 121550.

[34] ZHOU He-peng, XIE Fan-xin, ZHANG Yong-bing, ZHANG Bo-yuan, YANG Si-qi, LUO Xian-ping. Insights into the floatability between spodumene and albite from crystal chemistry standpoint [J]. International Journal of Mining Science and Technology, 2022, 32(6): 1329−1339.

[35] YELLA REDDY P, SRINIVASA KRISHNA T, GOWRISANKAR M, SIVA KUMAR K, KUMAR C N S S P. Acoustic, volumetric and FTIR study of binary liquid mixtures of 2-methyl cyclohexanone with amides [J]. The Journal of Chemical Thermodynamics, 2021, 154: 106316.

[36] RAKIPOV I T, PETROV A A, AKHMADIYAROV A A, KHACHATRIAN A A, VARFOLOMEEV M A. FTIR spectral study of intermolecular interactions of C═O groups of amides in solution [J]. Journal of Molecular Liquids, 2022, 354: 118838.

[37] SUN Wei, LAN Liu-jia, ZENG Hua, ZHOU Jian-fei, AHMED KHOSO S, WANG Li. Study on the flotation separation mechanism of diaspore from kaolinite using mixed NaOL/BHA collector [J]. Minerals Engineering, 2022, 186: 107719.

[38] ZHANG Hong-liang, XU Zhi-jie, SUN Wei, CHEN Dai-xiong, LI Sai, HAN Ming-jun, YU Heng, ZHANG Chen-yang. Selective adsorption mechanism of dodecylamine on the hydrated surface of hematite and quartz [J]. Separation and Purification Technology, 2021, 275: 119137.

金属离子和油酰肌氨酸钠对锂云母和长石浮选分离的协同作用机理

向国源[1]，范瑞华[1]，朱文韬[1]，孙 伟[1,2,3,4]，郑仁基[1,2,3,4]，高志勇[1,2,3,4]

1. 中南大学 资源加工与生物工程学院，长沙 410083；
2. 中南大学 战略含钙矿物资源清洁高效利用湖南省重点实验室，长沙 410083；
3. 中南大学 湖南省关键金属矿产资源高效清洁利用国际联合研究中心，长沙 410083；
4. 中南大学 金属资源开发利用碳减排教育部工程研究中心，长沙 410083

摘 要：将油酰肌氨酸钠与不同金属离子(Ca(II)、Mg(II)、Cu(II)和 Pb(II))组合，以提高锂云母和长石两种矿物的浮选分离效率。通过接触角测量、原子力显微镜、傅立叶变换红外光谱、药剂浓度组分分布计算和密度函数理论计算等手段研究该组合药剂的协同作用机理。结果表明，钙离子活化锂云母浮选的选择性最好。油酰肌氨酸钠在钙离子活化的锂云母表面的吸附能高达−1248.91 kJ/mol，而在钙离子活化的长石表面的吸附能低至−598.84 kJ/mol。因此，油酰肌氨酸钠和钙离子的组合药剂，在铝硅酸盐矿石中高效回收锂云母方面具有很好的应用前景。

关键词：浮选；锂云母；长石；油酰肌氨酸钠；金属离子

(Edited by Bing YANG)